

# Ortho-para transition rate in $\mu$ -molecular hydrogen and the proton's induced pseudoscalar coupling $g_p$

J.H.D. Clark<sup>1‡</sup> D.S. Armstrong<sup>1</sup> T.P. Gorringer<sup>2</sup> M.D. Hasinoff<sup>3</sup> P.M. King<sup>1°</sup> T.J. Stocki<sup>3◇</sup> S. Tripathi<sup>2</sup>  
D.H. Wright<sup>4†</sup> P.A. Zolnierczuk<sup>2\*</sup>

<sup>1</sup>College of William and Mary, Williamsburg, VA USA 23185 <sup>2</sup>University of Kentucky, Lexington, KY 40506

<sup>3</sup>University of British Columbia, Vancouver, B.C., Canada V6T 1Z1 <sup>4</sup>TRIUMF, Vancouver, BC, Canada, V6T 2A3  
(November 19, 2018)

We report a measurement of the ortho-para transition rate in the  $p\mu p$  molecule. The experiment was conducted at TRIUMF via the measurement of the time dependence of the 5.2 MeV neutrons from muon capture in liquid hydrogen. The measurement yielded an ortho-para rate  $\Lambda_{op} = (11.1 \pm 1.7 \pm 0.9) \times 10^4 \text{ s}^{-1}$  that is substantially larger than the earlier result of Bardin *et al.* We discuss the striking implications for the proton's induced pseudoscalar coupling  $g_p$ .

The protons's weak axial current is governed by the weak axial form factor  $F_A(q^2)$  and the induced pseudoscalar form factor  $F_P(q^2)$  and their corresponding coupling constants  $g_a = F_A(0)$  and  $g_p = F_P(-0.88m_\mu^2)$ . The values of the coupling constants and the  $q^2$  dependence of the form factors are determined by the proton's substructure and the underlying QCD dynamics. The approximate chiral symmetry of QCD implies a rigorous relationship between these constants that yields either  $g_p = (6.5 \pm 0.2) g_a$  or  $g_p = 8.2 \pm 0.2$  [1–4], and its experimental verification is an important test of low energy QCD.

The dominant uncertainty in extracting  $g_p$  from  $\mu$  capture in liquid  $H_2$  is the ortho-para transition rate  $\Lambda_{op}$  from the ortho ( $\ell = 1$ )  $p\mu p$  state to the para ( $\ell = 0$ )  $p\mu p$  state. This transition has been investigated theoretically by several authors [5–8]. It proceeds by Auger emission and its rate is a function of the electronic environment of the  $p\mu p$  molecule, most notably analogues of the neutral  $H_1$  atom  $[(p\mu p)^+e]$  and the charged  $H_3^+$  ion  $[(p\mu p)^+H_2]^+$ . The only published measurement of the rate  $(4.1 \pm 1.4) \times 10^4 \text{ s}^{-1}$  by Bardin *et al.* [9] is two standard deviations from the calculated rate  $(7.1 \pm 1.1) \times 10^4 \text{ s}^{-1}$  of Balakov *et al.* [6].

Given its importance in determining  $g_p$  we have performed a new measurement of the rate  $\Lambda_{op}$ . Both the Bardin *et al.* experiment [9] and the current experiment were based on the measurement of the time spectrum of the 5.2 MeV neutrons from  $\mu p \rightarrow n\nu$  capture. Because of the spin dependence of the capture rate, and the spin configurations of the  $\ell = 0, 1$  molecules, the rate  $\Lambda_{op}$  is encoded in the neutron time dependence. Neglecting the initial formation of ortho molecules, the time dependence is

$$N(t) \propto e^{-\Lambda_D t} (\Lambda_{PM} + (\Lambda_{OM} - \Lambda_{PM}) e^{-\Lambda_{op} t}), \quad (1)$$

where  $\Lambda_D$  is the muon disappearance rate and  $\Lambda_{OM}$  and  $\Lambda_{PM}$  are the ortho and para capture rates. Since  $\Lambda_D$  and the hyperfine ratio  $\Lambda_{OM}/\Lambda_{PM}$  are well established by experiment or theory, the rate  $\Lambda_{op}$  can be extracted from the neutron time spectrum.

Our experiment was conducted on the M9B muon channel at the TRIUMF cyclotron. Incoming muons were counted in a two-element plastic scintillator beam telescope. The larger scintillator  $S1$  ( $33 \times 33 \times 0.32 \text{ cm}^3$ ) registered particles emerging from the beam pipe and the smaller scintillator  $S2$  ( $10 \times 10 \times 0.16 \text{ cm}^3$ ) registered particles incident on the  $H_2$  flask. The target [10,11] comprised a cylindrical flask of length 15 cm and diameter 16 cm containing 2.7 liters of liquid  $H_2$  with  $4 \pm 2$  ppm deuterium contamination and  $< 1$  ppb contamination from  $Z > 1$  impurities. The target flask had Au front/side walls and a Cu back-plate and the surrounding vacuum vessel had cylindrical Ag walls and a mylar front window.

Outgoing neutrons were detected in a liquid scintillator counter array consisting of four counters ( $N2$ - $N5$ ) with diameters 12.7 cm and thicknesses 12.7 cm and one counter ( $N1$ ) with a diameter 12.7 cm and a thickness 5.1 cm. The scintillator materials were NE224 ( $N1$ ), NE213 ( $N4$ ) and BC501A ( $N2$ ,  $N3$ ,  $N5$ ) which permit  $n/\gamma$  discrimination by pulse-shape. Sandwiched between the neutron counters and the vacuum vessel were plastic scintillator veto counters ( $E1$ - $E5$ ) for identification of  $\mu$ -decay electrons.

Signals from each neutron counter were fed to pulse-shape discrimination modules [12]. The modules generated outputs indicating either a  $\gamma$ -ray trigger ( $G$ ) or a neutron trigger ( $N$ ) via the comparison of the integrated signals in a 420 ns prompt gate and a 52 ns delayed gate. To reduce the neutron trigger rate from mis-identified  $\gamma$ -rays/electrons we rejected those triggers accompanied by either a veto counter signal ( $\bar{E}$ ) or a large neutron counter signal ( $\bar{O}$ ). All events that fulfilled the neutron trigger ( $N \cdot \bar{E} \cdot \bar{O}$ ) and pre-scaled events that fulfilled the  $\gamma/e$  trigger ( $G$ ) were recorded. The pulse-shape data included both primary information from the pulse-shape modules (PSD1) and secondary information from a charge integrating ADC (PSD2). Histories of beam telescope hits and veto counter hits were recorded in a multihit TDC.

The experiment was conducted in four distinct data-sets and yielded a total of  $3.7 \times 10^{10}$   $\mu^-$  stops in liquid  $H_2$ . Empty target runs (yielding  $0.9 \times 10^9$   $\mu^-$  stops) and positive muon runs (yielding  $2.0 \times 10^9$   $\mu^+$  stops) were used for background studies. In sorting the data we applied cuts to separate the neutrons from  $\mu p$  capture, with energies 5.2 MeV and lifetimes  $\sim 2$   $\mu s$ , from backgrounds which included both mis-identified  $\gamma$ -rays from electron bremsstrahlung and neutrons from nuclear  $\mu$  capture, photo-nuclear reactions, accelerator sources, cosmic-rays, *etc.*

A pulse-shape cut and a pulse pile-up cut were used to minimize the contamination from mis-identified  $\gamma$ -rays. The pulse-shape cut involved a comparison of the integrated amplitudes in the signal peak and the signal tail, and used both PSD1 and PSD2 to achieve optimal n/ $\gamma$  discrimination. The pulse pile-up cut rejected any event with  $\geq 1$  neutron counter hits in a preceding 600 ns time window, such pile-up potentially distorting the n/ $\gamma$  discrimination.

An energy cut was used to enhance the signal of recoil protons from 5.2 MeV neutrons by requiring an energy equivalent of typically 2.5-5.0 MeV. A blank cut was used to reject the events from  $\mu$  capture in high-Z materials (*i.e.*  $\tau_{Au} = 73$  ns,  $\tau_{Ag} = 87$  ns and  $\tau_{Cu} = 163$  ns [13]) by rejecting any event with  $\geq 1$   $S1$  hits in a 400 ns window preceding the neutron. Finally, we used a duty cycle cut to reject any events occurring within 32  $\mu s$  of the beam-off period in the cyclotron time structure, and an errant muon cut to reject any events occurring within 5  $\mu s$  of an incoming beam particle that fired  $S1$  but missed  $S2$ .

The time spectra between incoming muons and detected neutrons for events that survived all cuts *excluding* the blank cut and all cuts *including* the blank cut are plotted in Fig. 1. Note that for each event we increment the time spectrum for every  $S1 \cdot S2$  coincidence in the multihit TDC. The spectra show a short-lifetime ( $\tau \sim 80$  ns) component that is most evident for events that failed the blank cut, a long-lifetime ( $\tau \sim 2$   $\mu s$ ) component that is only evident for events that passed the blank cut, and a continuum background. The short-lifetime component is dominated by Ag/Au capture, the long-lifetime component is dominated by  $H_2$  capture, and the continuum arises from uncorrelated muons.

The procedures for accounting for backgrounds in the time spectrum of the events passing all cuts were (i) subtraction of the continuum background from uncorrelated muons, (ii) determination of contributions from photo-nuclear reactions following electron bremsstrahlung, and (iii) the determination of contributions from  $\mu$  capture in low-Z materials.

The continuum is not perfectly time independent as decay electrons from uncorrelated muons can reject events by firing the veto counter ( $\overline{E}$ ) or overload circuit ( $\overline{O}$ ). This random vetoing of neutron events by uncorrelated muons can be seen as the shallow hole for  $t < 4$   $\mu s$

for events failing the blank cut. Note that for times  $t \gg \tau_{Au/Ag}$  the events failing the blank cut are entirely dominated by the continuum background while the events passing the blank cut are comprised of  $\mu p$  signal and continuum background. Thus, by normalizing and subtracting the events that failed the blank cut from those that passed the blank cut, the continuum is removed.

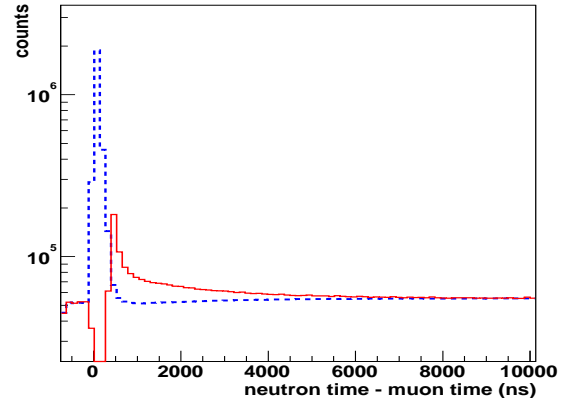


FIG. 1. Time spectra between incoming muons and detected neutrons for events that passed all cuts *except* the blank cut (dashed line) and all cuts *including* the blank cut (solid line). The shallow hole for  $t < 4$   $\mu s$  that's visible for events failing the blank cut is due to random vetoing. Note that  $t = -30$  to 370 ns corresponds to the blank cut and the dashed and solid curves are normalized at  $t > 10$   $\mu s$  region.

The photo-nuclear background originates from the photo-nuclear interactions [*e.g.*  $^{12}C(\gamma, p)$ ] in the liquid scintillators. Consequently, a tiny fraction of bremsstrahlung photons from decay electrons yield proton recoils. This background carries the 2.2  $\mu s$  lifetime of muonic  $H_2$  and therefore distorts the effective disappearance rate of  $\mu p$  capture neutrons. To measure this background we conducted a  $\mu^+$  measurement where neutrons from  $\mu$  capture are absent but those from photo-nuclear reactions are present. From the amplitude of the 2.2  $\mu s$  lifetime component in the  $\mu^+$  neutron time spectrum we determined a contribution of photo-nuclear interactions to  $\mu^-$  running that averaged about 14% for the thick counters N2-N5 but rose to  $55 \pm 8\%$  for the thin counter N1. We used a GEANT3 simulation [14] to account for the difference in the  $\gamma$ -ray spectra from  $\mu^+$  and  $\mu^-$  stops due to  $e^+$  annihilation.

The background from  $\mu$  capture in low-Z materials, *e.g.* scintillators, light-pipes, is worrisome as the muonic C and  $H_2$  lifetimes are similar (2.028  $\mu s$  and 2.195  $\mu s$ ). This background was determined by performing an empty target run in which  $\mu^-$  stops occur in the Cu back-plate not the liquid  $H_2$ . A GEANT3 simulation was used to establish that stops in scintillators, light guides, *etc.*, were dominated by scattering from the beam pipe window and

the beam telescope and thus unaffected by the target filling. The measurement showed no evidence for backgrounds from low-Z capture and established a limit of <7% on carbon backgrounds in production running.

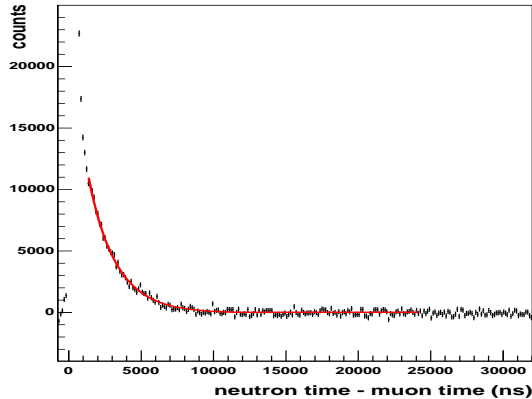


FIG. 2. Time spectrum of events that survive all cuts after the continuum subtraction. The points are the data and the solid curve is the benchmark fit.

The time spectrum of neutron events that survived all cuts, after the subtraction of the continuum, is plotted in Fig. 2. A typical energy spectrum ( $N4$ , data-set I) is plotted in Fig. 3. It shows the expected spectrum for 5.2 MeV neutrons as obtained by a GEANT3 simulation of the experimental set-up.

When muons stop in liquid  $H_2$  they evolve through a sequence of different atomic and molecular states. Also, if  $D_2$  is present other species of  $\mu$ -atoms and  $\mu$ -molecules are generated [15,16]. Therefore corrections were applied to Eqn. 1 to account for the  $p\mu p$  formation from the singlet  $\mu p$  atoms and the  $p\mu d$  formation due to  $D_2$  contamination. We assumed that, due to their typically lower energies, the efficiency for detecting neutrons from  $d/{}^3He$  capture is significantly smaller than the efficiency for detecting neutrons from proton capture, this making proton capture in  $p\mu d$  molecules the dominant correction from  $D_2$  contamination.

The determination of  $\Lambda_{op}$  was obtained by fitting to the Fig. 2 time spectrum. The fitting function was based on Eqn. 1, but supplemented with corrections accounting for  $p\mu p$  formation and  $D_2$  contamination. We also included a correction term with disappearance rate  $\Lambda_D$  to account for photo-nuclear backgrounds. In most fits we fixed the ratio  $\Lambda_{OM}/\Lambda_{PM} = 2.59$  [2,3] and rate  $\Lambda_D = 4.55 \times 10^5 \text{ s}^{-1}$  [19] at their known values and only varied the overall normalization and rate  $\Lambda_{op}$ .

Our benchmark fit (fit A) to all counters and all data-sets, which demonstrates the good agreement between the measured spectrum and the theoretical spectrum, is shown in Fig. 2. This yielded a rate  $\Lambda_{op} = (11.1 \pm 1.7) \times 10^4 \text{ s}^{-1}$  with a chi-squared *p.d.f.* of 1.03 for a fit range

of  $t = 1.3$  to  $24.3 \mu\text{s}$ , *i.e.* beginning beyond the region contaminated by Au/Ag capture.

The results of fits to study the sensitivity to backgrounds and corrections are listed in Table I. It shows that omitting the  $p\mu p$  formation correction (fit B) or  $p\mu d$  contamination (fit C) correction has little effect ( $< 1 \sigma$ ) on  $\Lambda_{op}$ . Including a 7% carbon background (fit D) changed the rate from  $(11.1 \pm 1.7) \times 10^4 \text{ s}^{-1}$  to  $(11.7 \pm 2.0) \times 10^4 \text{ s}^{-1}$ , a  $0.5 \sigma$  effect, while omitting the photo-nuclear background (fit E) changed the rate from  $(11.1 \pm 1.7) \times 10^4 \text{ s}^{-1}$  to  $(8.0 \pm 1.1) \times 10^4 \text{ s}^{-1}$ , a  $1.8 \sigma$  effect. Other tests indicated that varying the hyperfine ratio  $\Lambda_{OM}/\Lambda_{PM}$  by  $\pm 5\%$  changed the ortho-para rate  $\Lambda_{op}$  by  $\pm 4\%$ .

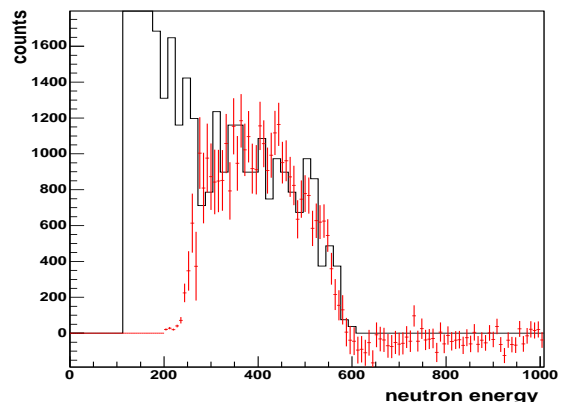


FIG. 3. Energy spectrum for counter  $N4$  and data-set I for events surviving all cuts with times  $t = 1.1$ - $3.3 \mu\text{s}$  after continuum subtraction. The points are the data and the histogram is the simulation. The data's upper edge (chan.  $\sim 550$ ) corresponds to 5.2 MeV proton recoils and the data's lower edge (chan.  $\sim 250$ ) results from the pulse-shape cut.

Also given in Table I are results from fits to the individual time spectra of the five neutron counters, thus demonstrating the consistency between counters. Similar checks of separate fits to the four different data-sets from the two running periods, which involved some differences in calibrations and settings, yielded results ranging from  $\Lambda_{op} = (10.3 \pm 2.6) \times 10^4 \text{ s}^{-1}$  to  $(13.7 \pm 3.0) \times 10^4 \text{ s}^{-1}$ . Lastly, we found no evidence of significant sensitivity to either the start-time or the end-time of the fit.

Several other tests of data integrity were performed. We sub-divided the neutron events into a low energy data-set (typically 2.5-3.7 MeV) and a high energy data-set (typically 3.7-5.0 MeV) and found consistent results for  $\Lambda_{op}$ . We analyzed the neutron events with energies  $> 5.2 \text{ MeV}$  and found no evidence for a long-lifetime component. Finally, the time spectrum of electron events yielded  $\tau = 2.198 \pm 0.002 \mu\text{s}$  and the time spectrum of empty-target neutron events yielded  $\tau = 163 \pm 1 \text{ ns}$ , consistent with the known values for the  $\mu p$  lifetime [19] and

the  $\mu\text{Cu}$  lifetime [13].

Our final result is  $\Lambda_{op} = (11.1 \pm 1.7_{\pm 0.6}^{0.9}) \times 10^4 \text{ s}^{-1}$  where the first error is statistical and the second error accounts for uncertainties in background determinations, chemistry corrections and  $\Lambda_{OM}/\Lambda_{PM}$  ( $\pm 5\%$ ). Our result is somewhat larger (by  $1.9 \sigma$ ) than the theoretical estimate  $\Lambda_{op} = (7.1 \pm 1.1) \times 10^5 \text{ s}^{-1}$  of Bakalov *et al.* [6] and substantially larger (by  $3.1 \sigma$ ) than the earlier measurement  $\Lambda_{op} = (4.1 \pm 1.4) \times 10^4 \text{ s}^{-1}$  of Bardin *et al.* [9].

In extracting  $g_p$  from  $\mu$  capture in liquid  $\text{H}_2$  the difference between  $\Lambda_{op} = 4.1 \times 10^4 \text{ s}^{-1}$  and  $11.1 \times 10^4 \text{ s}^{-1}$  is striking. With the Bardin *et al.* value  $\Lambda_{op} = 4.1 \times 10^4 \text{ s}^{-1}$  the TRIUMF RMC experiment [17,18] yields  $g_p = 12.2 \pm 1.1$  [17,18], the Saclay OMC experiment [19] yields  $g_p = 10.6 \pm 2.7$  [19], and the average value of the earlier liquid  $\text{H}_2$  experiments is  $g_p = 10.4 \pm 4.1$  [20,21], with the TRIUMF result being clearly inconsistent with theory. With the new measured value  $\Lambda_{op} = 11.1 \times 10^4 \text{ s}^{-1}$  the TRIUMF RMC experiment yields  $g_p = 10.6 \pm 1.1$ , the Saclay OMC experiment yields  $g_p = 0.8 \pm 2.7$ , and the average value of the earlier liquid  $\text{H}_2$  experiments yields  $g_p = 5.6 \pm 4.1$ , with the Saclay result being clearly inconsistent with theory.

The inconsistency between the present value for  $\Lambda_{op}$  and that measured by Bardin *et al.* is disconcerting. Note that an important difference between the two experiments is the beam time structure, the earlier work using a pulsed beam while the current work using a continuous beam. The experiments also differed in the total number of 5.2 MeV neutrons, the signal-to-noise for 5.2 MeV neutrons, and the presence in the Bardin *et al.* experiment of a long-lifetime background. However, we see no obvious explanation for the conflicting results.

Note that one consequence of the different time structures in the two experiments is the typical time between the parent muon and the detected neutron, in the relevant region of the time spectra, is greater in the Bardin *et al.* experiment than the current experiment. Therefore, at least in principle, it is possible that unconventional  $\mu$ -chemistry in liquid hydrogen could manifest itself as different neutron disappearance rates in the two experiments.

In summary, we report a determination of the  $p\mu p$  ortho-para rate from the time spectrum of the 5.2 MeV  $\mu p$  capture neutrons. Our result  $\Lambda_{op} = (11.1 \pm 1.7_{\pm 0.6}^{0.9}) \times 10^4 \text{ s}^{-1}$  is somewhat larger than the theoretical result of Bakalov *et al.* [6] and strikingly larger than the only previously published measurement [9]. The new result has dramatic consequences for the determination of the induced pseudoscalar coupling  $g_p$ .

We thank the TRIUMF cyclotron staff and TRIUMF target group for the operation of the cyclotron and the target. We also thank the National Science Foundation (USA), Natural Sciences and Engineering Research Council (Canada), and Jeffress Memorial Trust and the

William & Mary Endowment for their financial support.

<sup>†</sup> Present address: SLAC, P.O. Box 20450, Stanford, CA 94309.

<sup>‡</sup> Present address: American Physical Society, One Physics Ellipse, College Park, MD 20740.

<sup>\*</sup> Present address: Indiana University Cyclotron Facility, 2401 Milo B Sampson Lane, Bloomington, IN 47408.

<sup>◦</sup> Present address: University of Illinois at Urbana-Champaign, Urbana, IL, 61801.

<sup>◊</sup> Present address: Radiation Protection Bureau, Health Canada, 775 Brookfield Road, Ottawa, ON, Canada.

- [1] M.L. Goldberger and S.B. Treiman, Phys. Rev. **111**, 354 (1958).
- [2] V. Bernard, N. Kaiser and Ulf-G. Meissner, Phys. Rev. D **50**, 6899 (1994).
- [3] Harold W. Fearing, Randy Lewis, Nader Mobed, and Stefan Scherer, Phys. Rev. D **56**, 1783 (1997).
- [4] T.P. Gorringer and H.W. Fearing, Rev. Mod. Phys. **76**, 31 (2004).
- [5] Steven Weinberg, Phys. Rev. Lett. **4**, 575 (1960).
- [6] D.D. Bakalov *et al.*, Nucl. Phys. A **384**, 302 (1982).
- [7] M.P. Faifman and L.I. Men'shikov, Hyperfine Interactions **118**, 187 (1999).
- [8] S.S. Gershtein and A.V. Luchinsky, Phys. of Atomic Nuclei **65**, 102 (2002).
- [9] G. Bardin *et al.*, Phys. Lett. B **104**, 320 (1981).
- [10] D. Wright *et al.*, Nucl. Instrum. Methods **A320**, 249 (1992).
- [11] W. Bertl *et al.*, Nucl. Instrum. Methods Phys. Res. **A355**, 230 (1995).
- [12] J.R.M. Annand, Nucl. Instrum. and Methods **A262**, 371, (1987).
- [13] T. Suzuki, D.F. Measday, and J.P. Roalsvig, Phys. Rev. **C35**, 2212 (1987).
- [14] R. Brun *et al.* GEANT3(1986); CERN report no. DD/EE/84-1 (unpublished).
- [15] I.T. Wang *et al.* Phys. Rev. **139**, B1528 (1965).
- [16] C. Petitjean *et al.*, Muon Catal. Fusion **5/6**, 199 (1990/91).
- [17] G. Jonkmans *et al.*, Phys. Rev. Lett. **77**, 4512 (1996).
- [18] D. H. Wright, *et al.*, Phys. Rev. C **57**, 373 (1998).
- [19] G. Bardin *et al.*, Nucl. Phys. A **352**, 365, (1981).
- [20] E. Bleser *et al.*, Phys. Rev. Lett. **8**, 288 (1962).
- [21] J. E. Rothberg *et al.* Phys. Rev. **132**, 2664 (1963).

TABLE I. Results for the rate  $\Lambda_{op}$  from the fits to the continuum-subtracted time spectra. Values are given for both the summed spectrum of all neutron counters and the individual spectra of each neutron counter. See text for explanation of fits A,B, C, D and E. The units of  $\Lambda_{op}$  are  $\times 10^4 \text{ s}^{-1}$ .

Cntr.	Fit A.	Fit B	Fit C	Fit D	Fit E
All	11.1 $\pm$ 1.7	12.2 $\pm$ 1.8	11.6 $\pm$ 1.7	11.7 $\pm$ 2.0	8.0 $\pm$ 1.1
N1	7.2 $\pm$ 10.6	8.2 $\pm$ 11.1	7.7 $\pm$ 10.6	7.3 $\pm$ 10.9	2.2 $\pm$ 3.9
N2	13.8 $\pm$ 5.5	15.4 $\pm$ 5.6	14.4 $\pm$ 5.5	14.8 $\pm$ 6.5	8.3 $\pm$ 3.1
N3	8.9 $\pm$ 2.1	9.9 $\pm$ 2.3	9.4 $\pm$ 2.2	9.2 $\pm$ 2.3	7.1 $\pm$ 1.7
N4	14.6 $\pm$ 6.2	16.1 $\pm$ 6.7	15.1 $\pm$ 6.2	15.5 $\pm$ 7.3	10.3 $\pm$ 4.1
N5	12.2 $\pm$ 3.0	13.5 $\pm$ 3.0	12.7 $\pm$ 3.0	12.9 $\pm$ 3.4	10.6 $\pm$ 2.6